Nanoscale

Accepted Manuscript

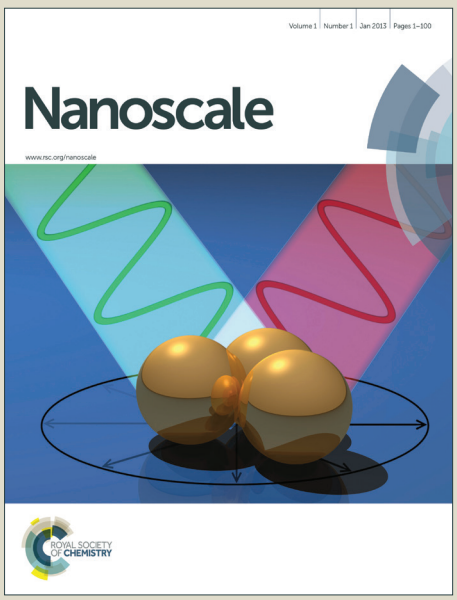

ROYAL SOCIETY OF CHEMISTRY

www.rsc.org/nanoscale

Journal Name

RSCPublishing

ARTICLE

A Facile and Versatile Method for Preparation of Colored TiO_2 with Enhanced Solar-Driven Photocatalytic Activity

Cite this: DOI: 10.1039/x0xx00000x

Received 00th January 2012,
Accepted 00th January 2012

DOI: 10.1039/x0xx00000x

www.rsc.org/

Huaqiao Tan, [a] Zhao Zhao, [ad] Mang Niu, [b] Chengyu Mao[c], Dapeng Cao, [b]* Daojian Cheng, [b] Pingyun Feng[c]* and Zaicheng Sun [a]*

Colored TiO_2 has attracted enormous attentions due to its visible light absorption and excellent photocatalytic activity. In this report, we develop a simple and facile solid-state chemical reduction approach for a large-scale production of colored TiO_2 at mild temperature (300-350 ^oC). The obtained sample possesses a crystalline core/amorphous shell structure (TiO_2@TiO_{2-x}). Oxygen vacancy results in the formation of disordered TiO_{2-x} shell on the surface of TiO_2 nanocrystals. XPS and theoretical calculation results indicate that valence band tail and vacancy band below conduction band minimum appear for the TiO_{2-x}, which implies that the TiO_2@TiO_{2-x} nanocrystal has a narrow band gap and therefore leads to a broad visible light absorption. Oxygen vacancy in a proper concentration promotes the charge separation of photogenerated carriers, which improves the photocatalytic activity of TiO_2@TiO_{2-x} nanocrystals. This facile and general method could be potentially used for large scale production of colored TiO_2 with remarkable enhancement in the visible light absorption and solar-driven H_2 production.

Introduction

Titanium dioxide (TiO_2), as the most widely used oxide semiconductors, has attracted considerable interest owing to its various applications in solar-driven hydrogen production, photocatalytic decomposition of pollutants, solar cells and so forth.[1-6] However, its photo-conversion efficiency is very limited owing to its large band gap energy (3.0 eV for rutile and 3.2 eV for anatase), which account for less than 2.2 % under AM 1.5 global solar illumination.[7, 8] Therefore, much effort has been made to enhance the visible and infrared light absorption of TiO_2 by band engineering including metal,[9-11] non-metal[12 13-15] and self-doping.[16-20] Recently, Mao *et al.* presented a breakthrough method to generate disordered nanophase TiO_2 and simultaneously incorporated a dopant through the hydrogenation of TiO_2 nanocrystals at 20 bar H_2 for 5 days. The black TiO_2 with a narrow band gap (≈ 1.54 eV) has been prepared, and exhibits extremely high photocatalytic activities for water splitting and dye degradation.[21] Since then, black TiO_2 attracted enormous attention.[22-29] Several synthesis routes including high pressure,[21] high temperature,[26] plasma assisted hydrogenation[27] and high temperature Al vapor reduction,[27] were developed. In Mao's report, black TiO_2 shows a great photocatalytic performance,[21] but high pressure synthesis route is less suitable for practical application. In addition to the above high pressure synthesis, amorphous TiO_2 can be transformed into black TiO_2 under high temperature (> 500 ^oC) and H_2 environment.[26] However, it is difficult to control the crystallite size of TiO_2 and its photocatalytic activities owing to the high temperature and long annealing process. And according to the report, this method is not applicable to crystalline TiO_2.[26] Recently, Huang et al. developed an aluminothermic reduction method for preparing black TiO_2.[27] However, high temperature (800 ℃ for producing aluminum vapor and 500 ℃ for the reaction) and long reaction times (6-20 h) were still required

There are two significant problems that impeded potential application of black TiO_2: Firstly, a facile and economical synthesis is highly demanded to produce black TiO_2 with excellent photocatalytic activity. Secondly, although many prominent works about black TiO_2 have been reported, it is still unclear about the mechanism of the formation of the disordered TiO_2. For example, it is not clear what happens to the structure and composition of TiO_2 that resulted in the disorder layer, and why such a modified surface enhances the photocatalytic activities of TiO_2.[23] In a word, there has been lack of systematic investigation on the nature of the surface change brought about by hydrogenation and reduction.

Herein, we have developed a facile and general method for large-scale production of colored TiO_2 through a controllable

solid-state reaction of $NaBH_4$ and crystalline TiO_2 (P25, anatase and rutile). With this approach, a series of colored TiO_2 from light blue via blue, dark blue and finally to black have been synthesized. By combining diverse characterization techniques and theoretical simulation, a plausible explanation on the color changes, appearance of disordered layer, enhanced photocatalytic activity, and the change of energy level and band gap of TiO_2 nanocrystals has been proposed. TEM results reveal that the nature of these colored titania has a crystalline core/amorphous shell structure feature (TiO_2@TiO_{2-x}). XPS and theoretical calculation results prove that the changing in energy level and associated band gap narrowing occur for the TiO_{2-x} shell owing to the emergence of the valence band tail and vacancy band below conduction band minimum, which results in the broad visible light absorption of TiO_2@TiO_{2-x} nanocrystals. On the other hand, oxygen vacancy in a certain concentration promotes the charge separation of photo-generated carriers leading to the improvement of photocatalytic performance. Among these samples, the optimal photocatalytic activity for H_2 production under UV-Vis irradiation is up to 6.5 mmol h^{-1} g^{-1}, which is about 7.2 times more than that of the original TiO_2 P25 (Degussa). Excess oxygen vacancy could serve as a charge recombination center, and lead to the decrease of photocatalytic activity. This observation provides a justification for the fact that the final black TiO_2 sample shows lower photocatalytic activity.

Experimental Section

Chemicals and materials

P25 was purchased from Degussa. Anatase (99.8 %, 25 nm), rutile (99.8 %, 25 nm) and $NaBH_4$ (98 %) were purchased from Aladdin Reagent Company. Ethanol (AR) was purchased from Beijing Chemical Reagent Company, and used as received without any further purification.

Preparation of colored TiO_2@TiO_{2-x}

At room temperature, the 4.0 g of TiO_2 nanoparticles powder (P25, anatase and rutile) was mixed with 1.5 g of $NaBH_4$ and the mixture was ground for 30 min thoroughly. Then the mixture was transferred into a porcelain boat, and placed in a tubular furnace, heated from room temperature to 300-400 ^oC under Ar atmosphere with a heating rate of 10 ℃ min^{-1} and then hold at designed temperature for 5 - 60 min. After naturally cooling down to room temperature, the colored TiO_2 was obtained, simply washed with deionized water and ethanol for several times to remove unreacted $NaBH_4$, and dried at 70 ℃. A series of different colored TiO_2 tuned from light blue to black can be prepared by controlling the reaction time and reaction temperature.

Characterizations

The crystalline structure was recorded by using an X-ray diffractometer (XRD) (Bruker AXS D8 Focus), using Cu Kα radiation (λ= 1.54056 Å). Transmission electron microscope (TEM) images were taken using an FEI Tecnai G2 operated at 200 kV. Scanning electron microscope (SEM) images were measured on a JEOL JSM 4800F. The UV–Vis absorption spectra were measured on a Shimadzu UV 2600 UV/Vis spectrophotometer. Raman spectra were collected on a Thermal Dispersive Spectrometer using a laser with an excitation wavelength of 532 nm at laser power of 10 mW. X-ray photoelectron spectrum (XPS) analyses were performed on an ESCALABMKII spectrometer with an Al-Kα (1486.6 eV) achromatic X-ray source. The EPR spectra were collected using a Bruker EMX-8 spectrometer at 9.36 GHz at 100 K.

UV-Vis light photocatalytic degradation

The UV light photocatalytic activity of the TiO_2 sample was evaluated by monitoring the decomposition of methyl orange in an aqueous solution under UV-Vis irradiation from a 300 W Xe lamp. Pyrex glass vessel was used as the photoreactor. TiO_2 sample (50 mg) was mixed with methyl orange solution (50 mL, 20 ppm, pH = 1). After stirring for 30 min in dark to reach the adsorption equilibrium, the solution was illuminated with a 300 W Xe lamp. The concentration of aqueous methyl orange was determined with a UV-Vis spectrophotometer by measuring peak intensity at 507 nm.

Photocatalytic H_2 generation

50 mg photocatalyst loaded with 1.0 wt. % Pt was placed into an aqueous methanol solution (120 mL, 25%) in a closed gas circulation system (Perfect Light Company Labsolar-Ⅲ (AG)). The UV light and visible light irradiations were obtained from a 300 W Xe lamp (Perfect Light Company Solaredge700) without and with a UVCUT-400 nm filter (Newport), respectively. Methanol was used as a sacrificial reagent. The amount of generated H_2 was determined with an online gas chromatography (Schimazu GC-2014c).

Calculations of electronic structures of TiO_2 and TiO_{2-x}

Density functional theory (DFT) [34] calculations were performed using the frozen-core all-electron projector-augmented-wave (PAW) [36, 37] method as implemented in the Vienna Ab-initio Simulation Package (VASP)[38, 39]. The Perdew-Burke-Ernzerhof (PBE) [40] parameterization of generalized gradient approximation (GGA) was adopted to describe the exchange and correlation potential. The cutoff energy for the plane-wave basis set is 500 eV. The 2×2×2 96-atom (32 Ti atoms and 64 O atoms) anatase supercell was used to construct a series of reduced TiO_2 systems with different reduced Ti-states, in which one, two and three of O atoms that neighboring one Ti centre atom of anatase supercell were removed to simulate one, two and three O vacancies, respectively. The geometry optimizations were carried out until the forces on each ion was reduced below 0.01 eV/Å, and the resulting structures were then used to start the calculations of electronic properties. Density of states (DOSs) calculations were performed using the Heyd-Scuseria-Ernzerhof (HSE06) hybrid functional, [41, 42] which can predict the correct electronic structures and defect levels of transition metal oxides such as TiO_2. In the HSE06

functional, the exchange contribution is divided into short- and long-ranged parts. The short-ranged part of PBE exchange is mixed with 25 % Hartree-Fock (HF) exchange. The Monkhorst-Pack[43] *k*-point mesh of 5×5×3 and 3×3×3 were used for the geometry optimizations and DOS calculations, respectively.

Results and Discussion

Structure Features and Physical Properties

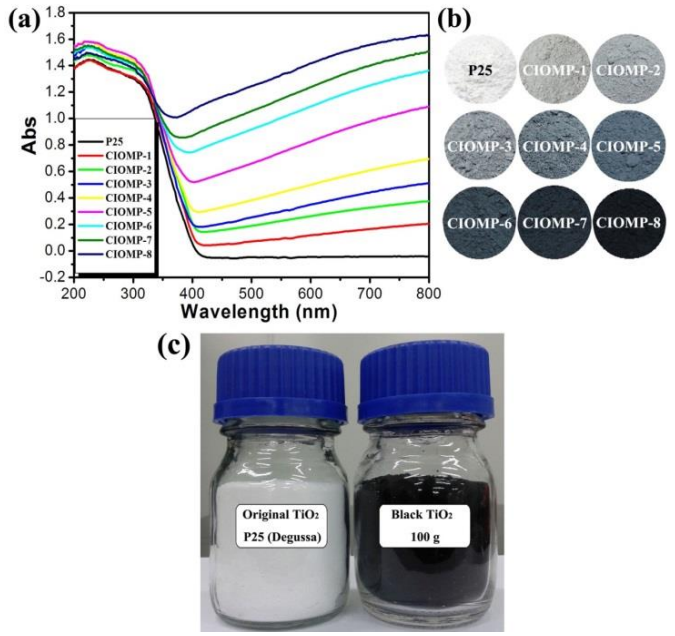

Figure 1. (a) The diffuse reflectance UV-Vis spectra of colored TiO_2; (b) Photographs of colored titania and pristine P25; (c) Large amount of black titania synthesized by $NaBH_4$ reduction route. CIOMP-1, treated at 300 °C 5 min; CIOMP-2, 300 °C 10 min; CIOMP-3, 300 °C 20 min; CIOMP-4, 300 °C 30 min; CIOMP-5, 300 °C 40 min; CIOMP-6, 300 °C 50 min; CIOMP-7, 300 °C 120 min; CIOMP-8, 350 °C 60 min.

To develop a facile and general synthesis route to prepare colored TiO_2 with visible light response, P25 TiO_2 nanocrystals were chosen as starting material. P25 TiO_2 nanocrystals were simply mixed with $NaBH_4$ powder by grinding, and then the mixture was transferred into tube furnace and heated up to 300 °C and hold for 5-120 minutes under argon atmosphere. The yield of colored TiO_2 is close to 90% based on the original TiO_2 amount. In this route, $NaBH_4$ decomposed at mild reaction temperature and *in situ* produced the active hydrogen, which is more reactive than H_2 and other reductants at this temperature in the previous reports. [18, 21, 24, 26-28] Strong reduced capability of active hydrogen is beneficial to carry out the reaction at relative short time and low temperature, which is helpful to maintain the original morphology of TiO_2 nanocrystals. Furthermore, different reduced degree of TiO_2 nanocrystals could be obtained by tuning the reaction conditions due to high reactivity of active hydrogen. That will help us understand the formation mechanism of reduced TiO_2. In addition, the byproducts from $NaBH_4$ can be easily removed by water and ethanol wash. The XPS results indicate that there is no B and Na residual (Figure S1).

As shown in Figure 1b, the color of TiO_2 turned from white to light blue and finally into dark blue with the increase of reaction time. When the reaction temperature rose up to 350 °C, the black TiO_2 could be obtained in 60 minutes. This series of samples were marked as CIOMP-n (n=1-8 for different reaction conditions, as shown in Figure 1). The corresponding diffuse reflectance UV-Vis spectra clearly show a broad absorption, starting at ~ 400 nm and extending in the near infrared (NIR) region of the spectrum. The intensity of the absorption band gradually increases with increasing the reaction time and temperature, which is consistent with the color change of the samples. In order to prove its generality and suitability for potential large-scale production, the colored anatase and rutile nanocrystals have also been prepared from pure anatase or rutile TiO_2 nanocrystals (as shown in Figure S2 - 5). And large amount of black titania have been synthesized through this simple synthesis route as shown in Figure 1c. The colored TiO_2 samples show high stability and almost negligible change at ambient conditions over a year (Figure S6).

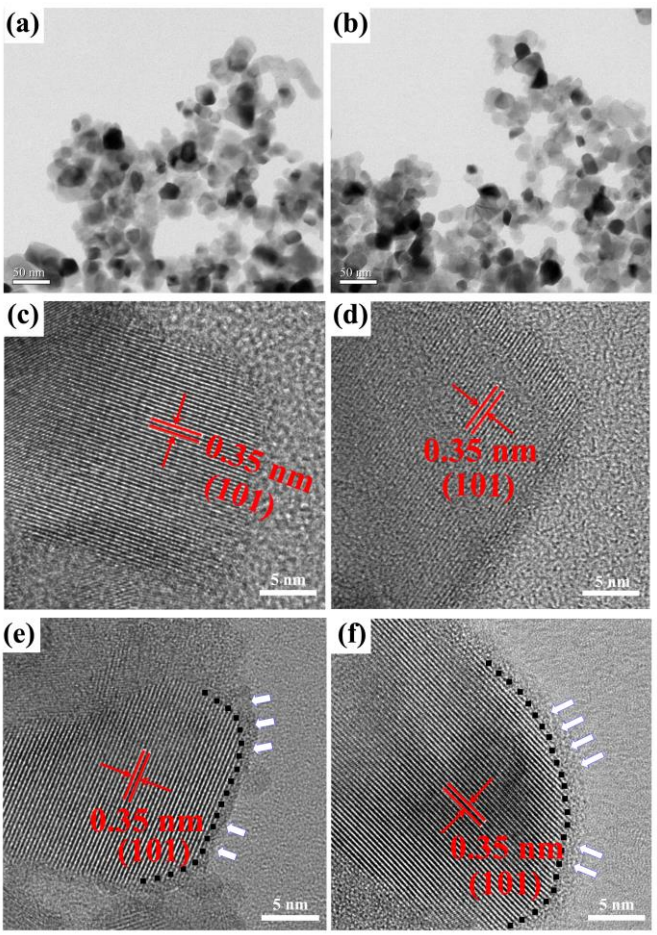

Figure 2. TEM images of titania nanocrystals before ((a): P25) and after ((b): CIOMP-8) reduction; (c–f) HRTEM images of TiO_2 nanocrystals P25 (c), CIOMP-2 (d), CIOMP-6 (e) and CIOMP-8 (f).

Scanning electron microscopy (SEM, Figure 2a, 2b and Figure S7) and transmission electron microscopy (TEM, Figure 2c – 2f) images reveal that the morphology and particle size of the TiO_2 nanocrystals before and after $NaBH_4$ treatment show no change. This could be further confirmed by the N_2 adsorption experiment (Figure S8). The BET specific surface areas for these colored titania (~ 43.86 m^2/g for CIOMP-4 and ~ 47.92 m^2/g for CIOMP-8) and pristine P25 (~ 45.04 m^2/g) indicate that the crystal sizes of pristine P25 do not change much during the treatment. This is further verified by our TEM results. As shown in Figure 2, TEM images reveal that the average diameter of TiO_2 nanocrystals is ~ 25 nm. High-resolution TEM (HR TEM) images provide detailed information on the structure of TiO_2 nanocrystals. Before the reduction treatment, TiO_2 nanocrystals exhibit highly crystalline nature and well-resolved lattice feature throughout the whole particles. Figure 2d shows HR TEM images of CIOMP-2 that is produced from P25 TiO_2 nanocrystals by reduction-treatment at 300 ^oC for 10 minutes. The TiO_2 nanocrystals show crystallized core with negligible disordered shell. When the treatment time extends to 50 minutes (CIOMP-6), a disordered layer with ~ 1.0 nm thickness is clearly observed in the HR TEM images (Figure 2e). When the treatment temperature rises up to 350 ^oC for 60 minutes, the disordered layer becomes thicker (Figure 2f). However, the core of nanocrystals is still highly crystalline. The lattice plane distances of crystalline core are 0.35 nm, which is the same as the lattice plane (101) of anatase TiO_2. The HR TEM results confirm that all these CIOMP-n samples have TiO_2@TiO_{2-x} core/shell structure feature. When the P25 sample is treated at 400 ^oC for 10 hours, a change in lattice plane occurs as shown in HR TEM images (0.37 nm, Figure S9), which indicates that new crystalline phases might have been formed during the treatment.

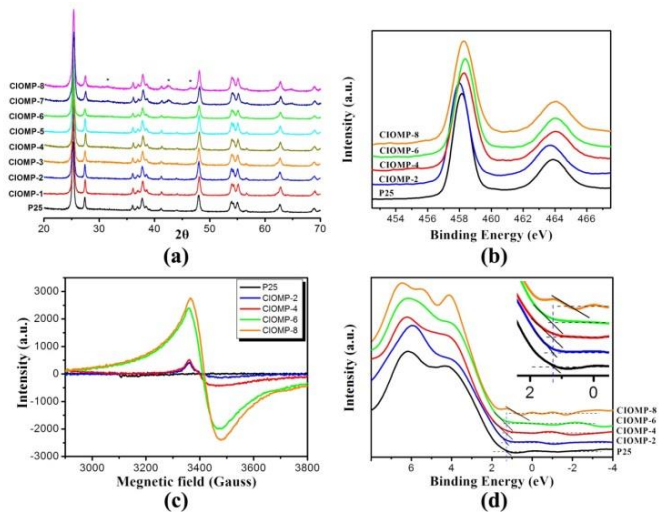

Figure 3. (a) XRD pattern of P25 and colored TiO2@TiO2-x samples; (b) Ti 2p XPS spectra; (c) EPR spectra of colored TiO2@TiO2-x and pristine TiO2; (d) Valence band XPS spectra of the pristine P25 and CIOMP-n.

The X-ray diffraction (XRD) is used to characterize the change of crystalline phase of TiO_2 nanocrystals. XRD patterns of CIOMP-n are illustrated in Figure 3a. The strong diffraction peaks indicate that CIOMPs are highly crystalline as pristine P25 TiO_2 (a mixture of anatase and rutile). However, a slightly broadening main peak is observed with increasing reaction time and temperature, which might be related to oxygen vacancies, as a result of disorder-induced lattice strains and slightly-reduced crystallite size. And three new peaks (marked with * in the Figure 3a) are also observed for longer reaction time (CIOMP-7, 300^oC for 120 minutes) and higher temperature (CIOMP-8, 350 ^oC for 60 minutes) reduction treatment, indicating that a new crystalline phase may have been formed. To better understand the origin of these three peaks, over-treated TiO_2 sample was obtained by reduction-treatment at 400 ^oC for 10 hours. The XRD pattern, as shown in Figure S10, exhibits a series of new peaks indicating that new crystalline phases were formed. This is consistent with TEM results. These new diffraction peaks cannot be matched to a known phase in the Powder Diffraction File (PDF) database, but they could be attributed to a mixture of several reduced titanium oxides such as Ti_9O_{17}, Ti_8O_{15}, Ti_3O_5. In short, oxygen vacancy was produced on the surface of TiO_2 nanocrystals through the chemical reduction treatment. With the increase of oxygen vacancy concentration, the long-range ordering of the crystal could be reduced, and the crystalline lattice deformation could occur, thus resulting in the formation of the disordered layer (TiO_{2-x}).

The oxygen deficiency and amorphous surface of TiO_{2-x} are unambiguously supported by Raman spectroscopy. As shown in Figure S11, there are six Raman active modes with frequencies at 144, 197, 399, 519, and 640 cm^{-1}, which indicated that these colored titania and pristine TiO_2 exhibit a typical anatase phase. With the increase of oxygen vacancy concentration in TiO_2 nanocrystals, the strongest Eg mode area at 144 cm^{-1} amplifies and exhibits a blue shift accompanied with peak broadening, compared with pristine TiO_2. As reported in the previous studies, the shift and broadening of the peaks of TiO_2 can be ascribed to the decrease of crystal domain size and nonstoichiometry.[27]

X-ray photoelectron spectroscopy (XPS) can provide useful information of chemical binding and valence band position on the sample surfaces. The high-resolution spectra of Ti 2p XPS and valence band of pristine P25, CIOMP-n and TiO samples are shown in Figure 3 and Figure S12. The Ti2p 3/2 and Ti 2p 1/2 peaks centered at binding energy 458.2 and 464.0 eV are typical characteristics of the Ti^{4+} - O bonds in P25 TiO_2. In the CIOMP-2, these peaks shift to low binding energies of 458.0 and 463.8 eV, which indicate that Ti^{3+} may have been formed in the CIOMP-2 sample as reported.[19, 27] The peak at 458.0 eV can be fitted into two Guassian peaks at 457.6 and 458.1 eV (Figure S12b), which can be assigned to Ti^{3+} and Ti^{4+}, respectively. With the increase of reaction time, the Ti characteristic peaks of CIOMP-4 shift back and to a little higher binding energy than that of pristine P25. The peak at 458.3 eV can be developed into 3 peaks at 457.7, 458.3 and 459.3 eV.

Compared with CIOMP-2, the peak intensity at 457.7 becomes weaker, which indicates that Ti^{3+} concentration decreases. Since the Ti 2p 3/2 peak of TiO (Figure S12f) can be fitted into three peaks at 456.2 (Ti^{2+} 2p 3/2), 458.2 and 459.7 eV (Ti^{2+} 2p 1/2),[30] the new peak observed at 459.3 eV could be caused by the increased oxygen vacancy concentration or the occurrence of lower valence Ti species like Ti^{2+} in TiO. The peak intensity at ~ 459.0 eV increases with the increase of reaction time and/or temperature, further suggesting the increased oxygen vacancy concentration. The whole process can be understood as the following. The reductant $NaBH_4$ decomposes under high temperature conditions, resulting in the formation of oxygen vacancy and reduced Ti sites such as Ti^{3+} and even lower oxidation state in the TiO_2 nanocrystals. This change in oxidation state is supported by the observed peak shift for Ti 2p to low binding energy and then to high binding energy. Electron paramagnetic resonance (EPR) spectra were further employed to confirm the above conjecture. As shown in Figure 3c, the EPR signal observed in CIOMP-n with g = 1.95 can be attributed to paramagnetic oxygen vacancies ($V_O^{\bullet}$) Ti^{3+}, and other lower valence Ti species, as documented for many oxide materials (e.g., Ta_2O_5, CeO_2, ZnO, etc.).[31] The signal intensity increases from CIOMP-2 to CIOMP-8, indicating that the oxygen vacancy concentration in CIOMP-n increases with the reaction process.

Figure 3d shows the valence band (VB) XPS of P25 and CIOMP samples. P25 displayed the characteristic VB density of states (DOS) with the band edge at ~1.26 eV below the Fermi energy.[26] Because the band gap of pristine P25 is 3.10 eV from the optical absorption spectrum, the conduction band minimum would occur at about -1.84 eV. The valence band maximum energy shows negligible change for the sample of CIOMP-2 to CIOMP-6. However, VB from XPS shows a blue-shift with the band tail about 0.76 eV in black CIOMP-8 sample. That indicates that the VB shift of CIOMP-8 has been caused by the reduction-treatment.

Photocatalytic Activity

The H_2 production from water under UV and visible light irradiations, as shown in Figure 4a, was used to evaluate the photocatalytic activity of P25 and CIOMP samples. 50 mg photocatalyst loaded with 1.0 wt. % Pt was placed into an aqueous methanol solution (120 mL, 25%) in a closed gas circulation system (Perfect Light Company Labsolar-III (AG)). The 300W Xe lamp was used as the UV - Visible light source. Pristine P25 steadily produced hydrogen gas at about 45 μmol h^{-1} for 0.05 g P25 (0.9 mmol h^{-1} g^{-1}). After it is treated with $NaBH_4$, the H_2 production rate of CIOMP samples was increased. For the dark blue CIOMP-6, the maximum H_2 production was up to 325 μmol h^{-1} for 0.05 g CIOMP-6 (6.5 mmol h^{-1} g^{-1}) under UV - Visible light irradiations, which is 7.2 times to that of pristine P25 and comparable to the reported excellent photocatalysts.[21, 27] The recycle experiments reveal that CIOMP-6 does not exhibit any reduction of photocatalytic activity for H_2 generation after eight photocatalysis cycles (Figure 4b). And under visible and infrared light irradiations, the rate of H_2-production for CIOMP-6 is about 9 μmol h^{-1} for 0.05 g CIOMP-6 (~180 μmol h^{-1} g^{-1}) (Figure 4c), which is almost consistent with previous references.[20, 22, 26, 27] However, as shown in Figure 4a, the rates of H_2 production under UV - visible light for CIOMP-7 and 8 are reduced to 215 and 115 μmol h^{-1} for 0.05 g sample (4.3 and 2.3 mmol h^{-1} g^{-1}), respectively, which might be related to the increase of oxygen vacancies in the TiO_2 nanocrystals. The oxygen vacancies were demonstrated to be electron donors in TiO_2[32] and considered to contribute to the enhanced donor density in hydrogenated TiO_2.[26] The increased donor density can improve charge transport in TiO_2 and shift the Fermi level of TiO_2 toward the conduction band.[33] Such a shift of the Fermi level can facilitate the charge separation at the semiconductor/electrolyte interface.

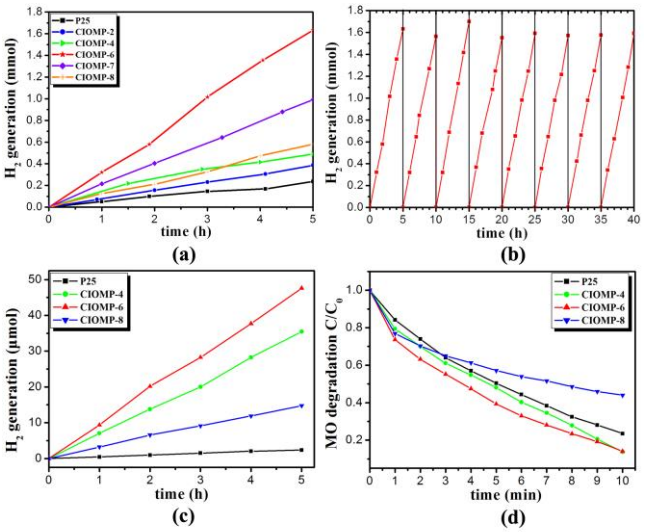

Figure 4. (a) Irradiation-time dependence of H_2 production over CIOMP-n and P25 under UV-Vis irradiations; (b) Recycling measure of hydrogen gas generation through photocatalytic water splitting with CIOMP-6 under UV-Vis irradiations; (c) Photocatalytic hydrogen generation with CIOMP-6 under visible light irradiations; (d) UV-Vis photocatalytic degradation of methylene orange.

Therefore, the enhanced charge separation and transportation are believed to be major reasons for the observed photocatalytic activity enhancement in CIOMP samples. However, when the concentration of the oxygen vacancy is too high, the defect can also act as charge recombination centers and lower free carrier mobility.[7] That could cause a negative effect on the photocatalytic performances,[7] which could be the reason why the photocatalytic activities in CIOMP-7 and 8 are reduced. The photocatalytic activities for the decomposition of methyl orange (MO) under UV-visible light irradiations were shown in Figure 4d and Figure S15. Photodegradation was completed after 10 minutes for CIOMP-6 (C/C_0 = 0.14), which was more effective than that of pristine P25 (C/C_0 = 0.24) under the same testing conditions.

Theoretical calculations

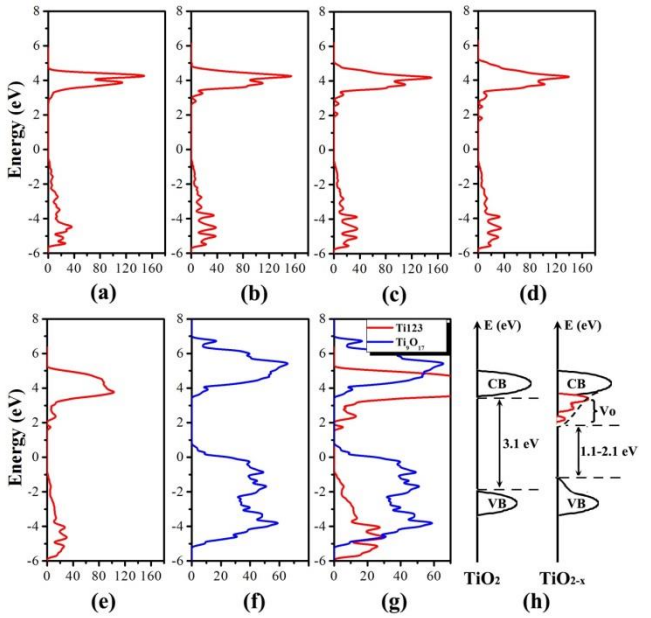

Figure 5. The Ti-3d DOS (a) pure anatase, (b)-(e) a series of theoretical simulation based on an anatase supercell $Ti_{32}O_{64}$: (b) one of Ti centre possess one oxygen vacancy; (c) one of Ti centre possess two oxygen vacancies; (d) one of Ti centre possess three oxygen vacancies; (e) a series of nonadjacent Ti centres which possess one, two and three oxygen vacancies, respectively (Ti123); (f) Ti_9O_{17}; (g) the stack of (e) and (f) used to simulate the Ti-3d DOS of the disorder layer which can be attributed to a mixture of a series of reduced titanium oxides; (h) Schematic electronic structures for TiO_2 and TiO_{2-x}.

In order to understand the origin of the change in optical and electronic properties of these colored TiO_2, a series of theoretical models have been constructed to mimic the TiO_{2-x} shell. All the models were calculated using the first-principles density functional theory (DFT).[34] As shown in **Figure 5**b-5d, the 2×2×2 96-atom (32 Ti and 64 O atoms) anatase supercell was selected to construct a series of reduced TiO_{2-x} systems, in which one, two and three of O atoms from one Ti center of anatase supercell were removed to simulate one, two and three O vacancies, respectively. The results of the Ti 3d DOS indicate that a new vacancy band appears below the conduction band (CB) minimum accompanied by the introduction of the oxygen vacancy. With the increase of oxygen vacancy concentration, the vacancy band shifts deeper and exhibits multiple bands at 0.5-1.5 eV below CB minimum, which is consistent with previous reports.[7, 32] In our case, the reduction reaction happens at a solid state, which may result in a non-uniform reaction. In another word, TiO_2 nanocrystals with 1, 2 and 3 oxygen vacancies may co-exist in our sample. Therefore, a model, in which a series of nonadjacent Ti centers possess one, two and three oxygen vacancies respectively, has been constructed and used to simulate the co-existing conditions. As shown in Figure 5e, a deep vacancy band at about 1.2 eV below CB minimum appears for the model. However, its VB exhibits no shift. Since we assume that there is no crystalline phase change in the model, these calculation results are consistent with our experimental results. In CIOMP-1~6, the XRD patterns (Figure 3a) show no crystalline phase changes. Their VB XPS spectra also show negligible shift (Figure 3d). In short, there is no influence on the TiO_2 VB by introducing oxygen vacancy when there is no crystalline phase change. Recently, some works[26, 35] reported that the oxygen vacancy may promote the transformation of TiO_2 nanocrystals from anatase to rutile phase at low temperature and reduction environment. As shown in Figure 3a, three new peaks were observed in the CIOMP-7 and 8 samples, indicating that new crystalline phase originated from disordered layer forms in the CIOMP-7 and 8 samples. Corresponding to the XRD pattern change, the VB tail was risen up in the VB XPS spectra of CIOMP-8 (Figure 3d). XRD results show that new diffraction peaks may origin from a mixture of a series of reduced TiO_2, for example, Ti_9O_{17}, Ti_8O_{15} and Ti_3O_5 etc. Therefore, the DOS of Ti_9O_{17} was also calculated. As shown in Figure 5f, the VB maximum rises up about 1.0-1.5 eV. That is to say, a risen up VB tail could be considered as the new reduced phase, which leads to a narrowed band gap and therefore improves visible light absorption.

Based on above experimental and theoretical results, the influence of oxygen vacancy on the energy level of anatase TiO_2 could be divided into two categories. One is that the crystalline phase of TiO_2 keeps in original phase, in which one or multiple vacancy bands appear below the CB minimum, but no change happens for VB. The narrowed band gap was obtained owing to existence of vacancy bands, which enhances the visible light response. The other is that the crystalline phase shows phase transformation. Accompanying with the change of crystalline phase, the VB of TiO_2 rises up, which also leads to a narrowed band gap. In our case, the above two stages should be in synergy. Figure 5e and 5f are superposed to simulate the reduced disordered layer (Figure 5g). The fallen CB tail and risen VB tail are observed, which makes the band gap narrowing to the range of 1.1-2.1 eV. The schematic electronic structures for TiO_2 and TiO_{2-x} disordered layer are shown in Figure 5h. In the reaction process, more oxygen atoms are removed from the TiO_2 surface, which shows the increase of oxygen vacancies with increasing reaction time. That is consistent with the fact that the EPR signal increases from CIOMP-2 to CIOMP-8. The color of CIOMP-n was darkened gradually, and the absorption for visible and infrared lights was enhanced. Since the vacancy band is a continuous band, the UV-Vis spectra of CIOMP-n show a broad absorption band in the range of 400-900 nm. Meanwhile, as the oxygen atoms are removed, the long-range order of crystal could be destroyed, and then the crystalline lattice deformation occurs, which thus results in the appearance of the disordered layer (TiO_{2-x}) and the change of electronic structures. Briefly, the oxygen vacancies can improve light absorption, promote the photo-generated charge separation and enhance the photocatalytic activity within a specific limit concentration (CIOMP-2~6). However, excess oxygen vacancy can also act as a recombination center for the photo-generate charges, and therefore result in the decrease of photocatalytic activity of TiO_2 in CIOMP-7 and 8 samples.

Conclusions

In summary, we have developed a new facile and general method for the synthesis of colored TiO_2 through a controllable solid state reaction. The method has the advantages of simple operation, low reaction temperature and short reaction time and provides an opportunity for massive production of high performance TiO_2 photocatalyst. By controlling reaction time and temperature, the color of TiO_2 can be tuned from light blue to blue, dark blue and finally to black. Such colored titania with a crystalline core/amorphous shell structure (TiO_2@TiO_{2-x}), possesses an enhanced visible light absorption capability. Their photocatalytic activities for water splitting hydrogen production and degradation of dyes have been improved significantly. The hydrogen production rate was up to 6.5 mmol h^{-1} g^{-1} under UV-visible light irradiations, which is 7.2 times higher than that of pristine P25. The color and surface changes of TiO_2 nanocrystals may result from the formation of oxygen vacancy. Results indicate that an optimum concentration of oxygen vacancy gives a maximum improvement of photocatalytic performance, beyond which the photocatalytic performance would decrease. Theoretical calculations and experimental results imply that the energy level of reduced TiO_{2-x} includes two categories: one is the CB tail owing to the appearance of vacancy bands; and the other is VB tail contributed from the TiO_2 crystalline phase transformation. These changes result in a narrow band gap, a broad visible light absorption and disordered layer.

Acknowledgements

The authors thank the National Natural Science Foundation of China (No. 21301166, 21201159, 61306081 and 61176016), Science and Technology Department of Jilin Province (No. 20130522127JH, and 20121801) and Returnee startup fund of Jilin is gratefully acknowledged. Z. S. thanks the support of the "Hundred Talent Program" of CAS, and the help from Prof. Jiesheng Chen and Prof. Guodong Li. The support from National Science Foundation (CHE- 1213795, P.F) is also greatly appreciated.

Notes and references

[a] State Key Laboratory of Luminescence and Applications, Changchun Institute of Optics, Fine Mechanics and Physics, Chinese Academy of Sciences, 3888 East Nanhu Road, Changchun 130033, People's Republic of China. Email: sunzc@ciomp.ac.cn

[b] Division of Molecular and Materials Simulation, State Key Laboratory of Organic-Inorganic Composites, Beijing University of Chemical Technology, Beijing 100029, People's Republic of China. Email: caodp@mail.buct.edu.cn

[c] Department of Chemistry, University of California, Riverside, California 92521, U. S. A. Email: pingyun.feng@ucr.edu

[d] University of Chinese Academy of Sciences, No.19A Yuquan Road, Beijing 100049, People's Republic of China.

Electronic Supplementary Information (ESI) available: More XRD, UV-Vis spectra, XPS, SEM, TEM and photocatalytic degradation of MO. See DOI: 10.1039/b000000x/

1. A. Fujishima and K. Honda, *Nature*, 1972, **238**, 37-38.
2. M. Graetzel, R. A. J. Janssen, D. B. Mitzi and E. H. Sargent, *Nature*, 2012, **488**, 304-312.
3. X. Chen and S. S. Mao, *Chem. Rev.*, 2007, **107**, 2891-2959.
4. X. Chen, S. Shen, L. Guo and S. S. Mao, *Chem. Rev.*, 2010, **110**, 6503-6570.
5. K. Nakata and A. Fujishima, *J. Photochem. Photobio. C: Photochem. Rev.*, 2012, **13**, 169-189.
6. Z. Zou, J. Ye, K. Sayama and H. Arakawa, *Nature*, 2001, **414**, 625-627.
7. R. Su, R. Tiruvalam, Q. He, N. Dimitratos, L. Kesavan, C. Hammond, J. A. Lopez-Sanchez, R. Bechstein, C. J. Kiely, G. J. Hutchings and F. Besenbacher, *ACS Nano*, 2012, **6**, 6284-6292.
8. A. B. Murphy, P. R. F. Barnes, L. K. Randeniya, I. C. Plumb, I. E. Grey, M. D. Horne and J. A. Glasscock, *Int. J. Hydrogen Energy*, 2006, **31**, 1999-2017.
9. M. R. Hoffmann, S. T. Martin, W. Choi and D. W. Bahnemann, *Chem. Rev.*, 1995, **95**, 69-96.
10. W. Choi, A. Termin and M. R. Hoffmann, *Angew. Chem. Int. Ed.*, 1994, **33**, 1091-1092.
11. W. Choi, A. Termin and M. R. Hoffmann, *J. Phys. Chem.*, 1994, **98**, 13669-13679.
12. R. Asahi, T. Morikawa, T. Ohwaki, K. Aoki and Y. Taga, *Science*, 2001, **293**, 269-271.
13. J. H. Park, S. Kim and A. J. Bard, *Nano Lett.*, 2005, **6**, 24-28.
14. S. U. M. Khan, M. Al-Shahry and W. B. Ingler, *Science*, 2002, **297**, 2243-2245.
15. X. Chen and C. Burda, *J. Am. Chem. Soc.*, 2008, **130**, 5018-5019.
16. J. Wang, D. N. Tafen, J. P. Lewis, Z. Hong, A. Manivannan, M. Zhi, M. Li and N. Wu, *J. Am. Chem. Soc.*, 2009, **131**, 12290-12297.
17. K. Xie, N. Umezawa, N. Zhang, P. Reunchan, Y. Zhang and J. Ye, *Energy Environ. Sci.*, 2011, **4**, 4211-4219.
18. F. Zuo, L. Wang, T. Wu, Z. Zhang, D. Borchardt and P. Feng, *J. Am. Chem. Soc.*, 2010, **132**, 11856-11857.
19. F. Zuo, K. Bozhilov, R. J. Dillon, L. Wang, P. Smith, X. Zhao, C. Bardeen and P. Feng, *Angew. Chem. Int. Ed.*, 2012, **51**, 6223-6226.
20. Q. Kang, J. Cao, Y. Zhang, L. Liu, H. Xu and J. Ye, *J. Mater. Chem. A*, 2013, **1**, 5766-5774.
21. X. Chen, L. Liu, P. Y. Yu and S. S. Mao, *Science*, 2011, **331**, 746-750.
22. X. Chen, L. Liu, Z. Liu, M. A. Marcus, W.-C. Wang, N. A. Oyler, M. E. Grass, B. Mao, P.-A. Glans, P. Y. Yu, J. Guo and S. S. Mao, *Sci. Rep.*, 2013, **3**, 1510.
23. Z. Zheng, B. Huang, J. Lu, Z. Wang, X. Qin, X. Zhang, Y. Dai and M.-H. Whangbo, *Chem. Commun.*, 2012, **48**, 5733-5735.
24. G. Wang, H. Wang, Y. Ling, Y. Tang, X. Yang, R. C. Fitzmorris, C. Wang, J. Z. Zhang and Y. Li, *Nano Lett.*, 2011, **11**, 3026-3033.
25. S. Hoang, S. P. Berglund, N. T. Hahn, A. J. Bard and C. B. Mullins, *J. Am. Chem. Soc.*, 2012, **134**, 3659-3662.
26. A. Naldoni, M. Allieta, S. Santangelo, M. Marelli, F. Fabbri, S. Cappelli, C. L. Bianchi, R. Psaro and V. Dal Santo, *J. Am. Chem. Soc.*, 2012, **134**, 7600-7603.

27. Z. Wang, C. Yang, T. Lin, H. Yin, P. Chen, D. Wan, F. Xu, F. Huang, J. Lin, X. Xie and M. Jiang, *Adv. Funct. Mater.*, 2013, DOI:10.1002/adfm.201300486.
28. Z. Wang, C. Yang, T. Lin, H. Yin, P. Chen, D. Wan, F. Xu, F. Huang, J. Lin, X. Xie and M. Jiang, *Energy Environ. Sci.*, 2013, **6**, 3007-3014.
29. L. Liu, P. Y. Yu, X. Chen, S. S. Mao and D. Z. Shen, *Phys. Rev. Lett.*, 2013, **111**, 065505.
30. T. Hanawa, *J. Periodontal Implant Sc.*, 2011, **41**, 263.
31. Y. Su, J. Lang, L. Li, K. Guan, C. Du, L. Peng, D. Han and X. Wang, *J. Am. Chem. Soc.*, 2013, **135**, 11433-11436.
32. A. Janotti, J. B. Varley, P. Rinke, N. Umezawa, G. Kresse and C. G. Van de Walle, *Phys. Rev. B*, 2010, **81**, 085212.
33. D. C. Cronemeyer, *Phys. Rev.*, 1959, **113**, 1222-1226.
34. P. Hohenberg and W. Kohn, *Phys. Rev.*, 1964, **136**, B864-B871.
35. M. Salari, K. Konstantinov and H. K. Liu, *J. Mater. Chem.*, 2011, **21**, 5128-5133.
36. P. E. Blöchl, *Phys. Rev. B*, 1994, **50**, 17953-17979.
37. G. Kresse and D. Joubert, *Phys. Rev. B*, 1999, **59**, 1758-1775.
38. G. Kresse and J. Hafner, *Phys. Rev. B*, 1994, **49**, 14251-14269.
39. G. Kresse and J. Furthmüller, *Phys. Rev. B*, 1996, **54**, 11169-11186.
40. B. Hammer, L. B. Hansen and J. K. Nørskov, *Phys. Rev. B*, 1999, **59**, 7413-7421.
41. J. Heyd, G. E. Scuseria and M. Ernzerhof, *J. Chem. Phys.*, 2003, **118**, 8207-8215.
42. J. Paier, M. Marsman, K. Hummer, G. Kresse, I. C. Gerber and J. G. Ángyán, *J. Chem. Phys.*, 2006, **124**, 154709.
43. H. J. Monkhorst and J. D. Pack, *Phys. Rev. B*, 1976, **13**, 5188-5192.

Table of content

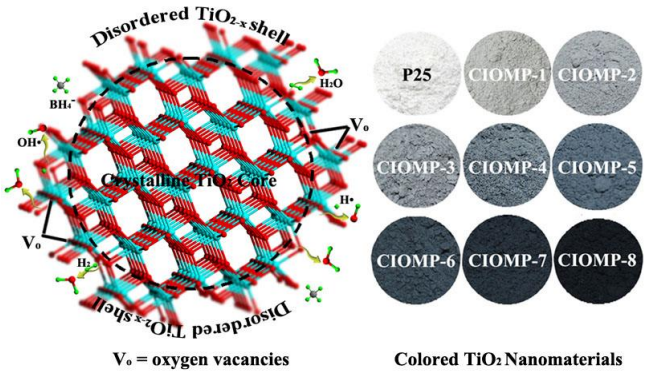

A simple and facile solid-state chemical reduction approach for a large-scale production of colored TiO_2 with good photocatalytic properties was developed.

